

## Analysis of soil resistance on drilled shafts using proposed cyclic $p$ - $y$ curves in weathered soil

Sangseom Jeong <sup>1a</sup>, Jeongsik Park <sup>1b</sup>, Junyoung Ko <sup>\*2</sup> and Byungchul Kim <sup>3c</sup>

<sup>1</sup> Department of Civil and Environmental Engineering, Yonsei University,  
50 Yonsei-ro, Seodaemun-gu, Seoul 03722, Republic of Korea

<sup>2</sup> Department of Civil, Environmental, and Construction Engineering, Texas Tech University,  
911 Boston Ave., Lubbock, TX 79409, USA

<sup>3</sup> Overseas Civil Project Management Team, Daelim Industrial Co.,  
36, Jong-ro 1-gil, Jongno-gu, Seoul 03152, Republic of Korea

(Received May 14, 2016, Revised November 16, 2016, Accepted November 18, 2016)

**Abstract.** A fundamental study of drilled shafts-soil systems subjected to lateral cyclic loading in weathered soil was conducted using numerical analyses. The emphasis was on quantifying the soil resistance of laterally cyclic loaded pile using 3D finite element analysis. The appropriate parametric studies needed for verifying the cyclic  $p$ - $y$  characteristic are presented in this paper. A framework for determining the cyclic lateral load transfer curve ( $p$ - $y$  curves) on the basis of numerical analyses is proposed. Through comparisons with results of field load tests, the three-dimensional numerical methodology in the present study is in good agreement with the general trend observed by in situ measurements and thus, represents a realistic soil-pile interaction for laterally loaded piles in soil than that of existing  $p$ - $y$  method. It can be said that a rigorous present analysis can overcome the limitations of existing cyclic  $p$ - $y$  methods to some extent by considering the effect of realistic three-dimensional combination of pile-soil forces. The proposed cyclic  $p$ - $y$  curve is shown to be capable of predicting the behavior of the drilled shafts in weathered soil.

**Keywords:** drilled shafts; lateral cyclic load; cyclic  $p$ - $y$  curves; 3D finite element method; weathered soil

### 1. Introduction

The behavior of the foundations under cyclic loading is important considering in design. Several empirical and numerical methods have been proposed for analyzing the load-deformation behavior of driven piles subjected to a vertically static loading; much less work has been done on laterally static loading, *let alone* cyclic or dynamic drilled shaft head loading. However, structure, such as buildings, bridges and offshore platforms are exposed to significant cyclic lateral loads in many situations including environmental loadings (wind, water, and earthquakes) and machine loadings. Among various methods of modelling a soil-pile system for cyclic lateral load, an equivalent soil-spring model using  $p$ - $y$  curves which can consider nonlinear soil behavior is most

---

\*Corresponding author, Ph.D., Post-Doc Research Associate, E-mail: [junyoung.ko@ttu.edu](mailto:junyoung.ko@ttu.edu)

<sup>a</sup> Ph.D., Professor, E-mail: [soj9081@yonsei.ac.kr](mailto:soj9081@yonsei.ac.kr)

<sup>b</sup> Ph.D. Student, E-mail: [hlpcs@hanmail.net](mailto:hlpcs@hanmail.net)

<sup>c</sup> Ph.D., Senior manager, E-mail: [bck@daelim.co.kr](mailto:bck@daelim.co.kr)

widely used in engineering practice.

The cyclic or dynamic loading can be representatively categorized according to the frequency and period. El Naggar and Bentley (2000) reported that the ranges of frequency were different in terms of the loading types, as shown Table 1.

Yang *et al.* (2009) performed the experimental tests to investigate the behavior of structures subjected to seismic loading using the shaking table. They reported that the frequency caused by the soil moving and internal force of superstructure represented from 10 to 20 Hz. Therefore, it is found that the cyclic loading has the low frequency, while the dynamic loading has the high frequency generally. On the other hand, for the period, the period of dynamic loadings such as the impact loading and seismic loading is very short, whereas those of cyclic loading is relatively long.

For the frequency effect on the behavior between soil and piles in sandy soil, the soil resistance under cyclic loading decreases typically (Reese *et al.* 1974). Long and Vanneste (1994) reported that the soil resistance under cyclic loading was influenced by the number of cycles, magnitude and types of cyclic loading, also, Lin and Liao (1999) and Verdure *et al.* (2003) stated that the behavior between soil and piles was not influenced by the frequency of cyclic loading. However, the soil resistance under dynamic loading increases due to the damping effect. Especially, El Naggar and Bentley (2000) described that the dynamic  $p$ - $y$  curves depended on the frequency. In summary, the soil resistance under cyclic loading decreases, whereas those under dynamic loading increase. Also, it is found that the dynamic  $p$ - $y$  curves depend on the frequency, but not the cyclic  $p$ - $y$  curves. The differences between cyclic and dynamic loadings are summarized in Table 2.

In this study, it is defined that the applied cyclic loads of field load tests and numerical analyses have the long period and low frequency. Also, as mentioned above, the cyclic  $p$ - $y$  curves was not influenced by the frequency of cyclic loading, thus, the frequency effect was not considered in this study.

Much work has been done to study static or cyclic  $p$ - $y$  curves by many researchers. In addition, static or cyclic  $p$ - $y$  curves have been proposed for analyzing the load-deformation behavior of piles subjected to a lateral loads. These methods make slightly different methodologies that can generally be classified into three groups: (1) empirical method (Broms 1964, Kim *et al.* 2014,

Table 1 Typical frequency ranges with loading types (El Naggar and Bentley 2000)

Loading types	Ranges of frequency
Earthquake	0 – 10 Hz
Offshore environmental loading	0 – 1 Hz
Machine foundations	5 – 200 Hz

Table 2 Differences between cyclic and dynamic loadings

Loading types	Cyclic loading	Dynamic loading
Cause of loading	Wind, wave, current	Earthquake, machine vibration, impact
Period	Long period, continuously	Short period, instantaneously
Frequency	Low frequency	High frequency
Influence factor on $p$ - $y$ curves	Number, magnitude and types of cycles	Frequency, magnitude of loading
Soil resistance	Decrease	Increase

2015, McCarron 2016), (2) experimental method (Matlock 1970, Reese *et al.* 1974, Murchison and O'Neill 1984, Ashour and Norris 2000, Kim and Jeong 2011), and (3) numerical method (NCHRP 2001, Achmus *et al.* 2009, Bourgeois *et al.* 2010, Memarpour *et al.* 2012, Damagaard *et al.* 2014, Liu *et al.* 2014).

These  $p$ - $y$  curves have been established for different soil conditions based on in situ pile tests under static or cyclic pile-head loadings (Matlock 1970, Reese *et al.* 1974, Murchison and O'Neill 1984, Ashour and Norris 2000, Kim and Jeong 2011). The cyclic  $p$ - $y$  curves proposed by Reese *et al.* (1974) were developed to represent the resistance provided by the soil at a large number of cycles of load. To determine the effect of cyclic lateral loads on piles, 34 full-scale tests were conducted in sand soil by Long and Vanneste (1994). The test findings indicated that the most important parameters were the characteristics of the cyclic load, the number of cycles, the method of installation and the soil density. The modified  $p$ - $y$  curves for static loading conditions are frequently extended to account for cyclic loading conditions without further verification because the cyclic  $p$ - $y$  curves have not been well established (Yang *et al.* 2009). Over the years, a number of researchers (Memarpour *et al.* 2012, Achmus *et al.* 2009) have attempted to propose models to explain the behavior of pile foundations under cyclic lateral load. However, those models were developed empirically and still had limitations. Therefore, a new cyclic  $p$ - $y$  curve is needed to evaluate the behavior of the pile under cyclic conditions.

This study presents a lateral cyclic load-transfer curve to take into account realistic soil-pile interaction through a series of 3D FE analysis. In this study, the soil resistance for a pile subjected to lateral loads was computed directly by integrating the stresses in the soil elements around the circumference of the pile. The modelling techniques and analysis results were validated using field measurements of lateral load tests performed at the test sites in South Korea. Based on numerical analysis, a modified lateral load transfer relationship and design chart with reduction factors were proposed by considering the characteristics of cyclic loading.

## 2. 3D finite element modelling

### 2.1 FE mesh and boundary conditions

A 3D FE model to investigate the response of a single pile under cyclic lateral loads in weathered soil is presented here. A commercial finite-element package, ABAQUS 6.13 (2013) was used for this study. The load does not occur in the  $y$ -direction, a half domain was adopted. The overall dimensions of the model boundaries comprise a width of 40 times the pile diameter ( $D$ ) from the pile center. The height is equals to the pile length ( $L$ ) plus a further  $1.25L$  below the pile-top level. These dimensions were considered adequate to eliminate the influence of boundary effects on the pile performance. Fig. 1 shows a typical 3D FE mesh applied to analyze a pile subjected to cyclic lateral loads.

The side boundary of the mesh was imposed to be on rollers to allow only downward movement and symmetric boundary. The bottom boundary of the mesh is fixed against displacements. The pile and soil were modeled with the C3D8R element, which specifies an 8-node linear brick, reduced integration with hourglass control.

### 2.2 Material FE mesh and boundary conditions

The surrounding soil layer is described by a linearly elastic-perfectly plastic constitutive law

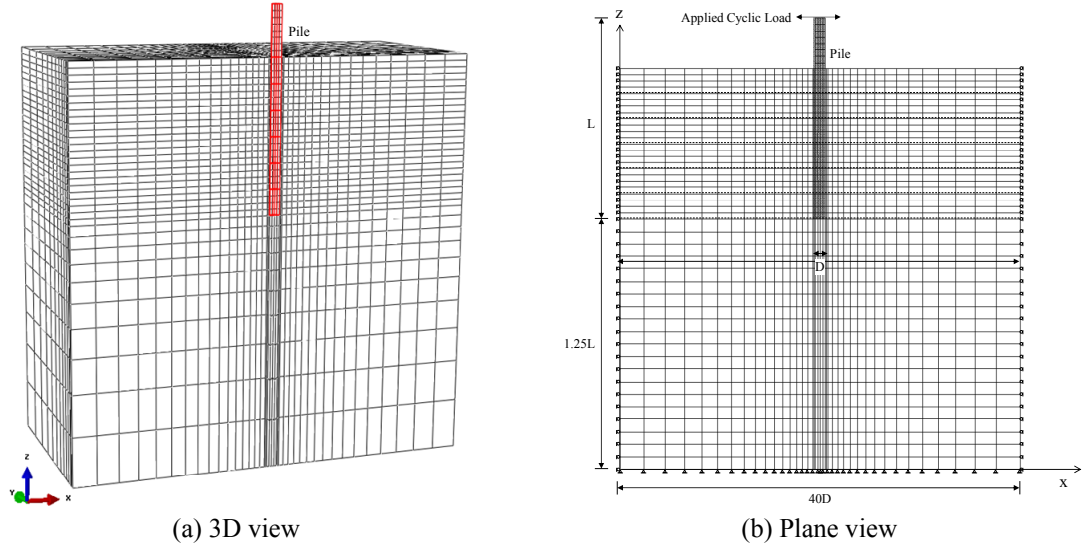


Fig. 1 Typical mesh and boundary conditions

using the Drucker-Prager model. The pile is considered as a linearly elastic material at all times. The dilation angle ( $\psi$ ) in the Drucker-Prager model was assumed to be half of the angle of friction to avoid unrealistically high dilation that takes place in the classical Drucker-Prager model due to the normality rules (Hassan and O'Neill 1997, Drumm *et al.* 2005).

To consider the initial equilibrium state, specified initial stress distributions were calculated based on the self-weight of the material. After the initial step, cyclic lateral loading was applied at the top of the pile. The modeling of the pile installation process is omitted; thus, the effect of the pile installation is ignored. In this study, the interface element modeled by the Coulomb's frictional model is employed to simulate the interface for a contact. This model is available in ABAQUS (2013). The shear behavior in the interface is that elastic behavior has going on until critical shear stress ( $\tau_{crit}$ ) in Eq. (1) reached and after that only shear displacement increases without increase of shear stress. The interface friction coefficient is adopted as 0.5 for concrete-soil interface.

$$\tau_{crit} = \mu \times p_c \quad (1)$$

where  $\mu$  is friction coefficient and  $p_c$  is contact pressure.

In addition, the bending moment is computed using the vertical stress from the finite element analyses as shown in Fig. 2. The bending moment can be calculated as follows

$$M = \frac{\sigma_{avg}}{y} I \quad (2)$$

$$\sigma_{avg} = \frac{(\sigma_{33,1} - \sigma_{33,2})}{2} \quad (3)$$

where  $M$  is the bending moment,  $y$  is the distance from center of pile to element centroid,  $I$  is the moment of inertia, and  $\sigma_{33,1}$  and  $\sigma_{33,2}$  are the vertical stress at element centroid, respectively.

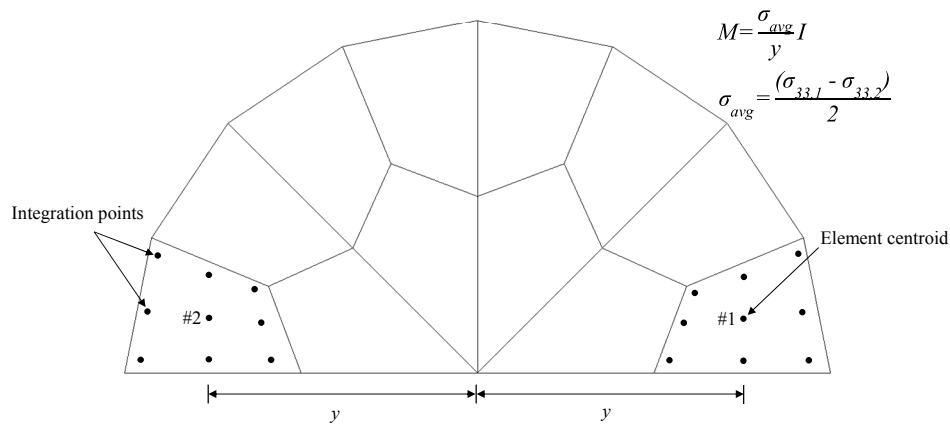


Fig. 2 Calculation of bending moment from finite element analyses

### 3. Validation by performing field load tests

#### 3.1 Site investigation

In this study, field tests were conducted to verify the FE model in Eumseong-gun, Chungcheongbuk-do, South Korea. This investigation was performed on three boreholes (BH-1, BH-2, BH-3) using conventional sampling near the test piles. The in situ field test included the standard penetration test (SPT), pressure meter test (PMT) and lateral load testing (LLT). Fig. 3 shows the location of the borings in relation to the test piles. The SPT results indicate that weathered soil deposits at 0.3–12 m were in a dense state. The SPT  $N$  values at these depths ranged from 16 to 50/30. According to the Unified Soil Classification System (USCS), the weathered soil is classified as silty sand (SM). The soil properties based on these site investigations are summarized in Table 3 and Table 4. A generalized soil profile for this site is presented in Fig. 4.

#### 3.2 Test piles and instrumentation

A schematic representation of the loading system for the cyclic load test is shown in Fig. 5. The instruments used for the cyclic load test included a hydraulic jack, a load cell and beams. The

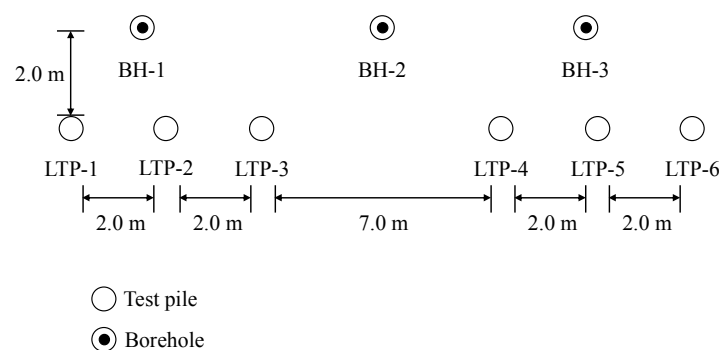


Fig. 3 Site plan with locations on field tests

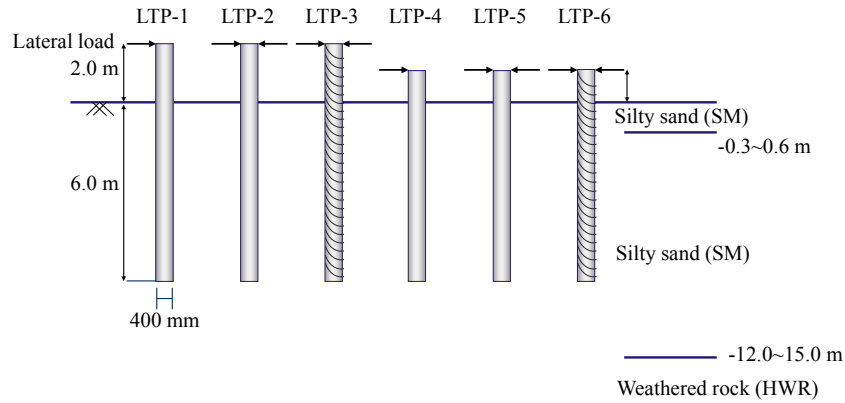


Fig. 4 Soil profile with borehole and embedment for test piles

Table 3 Results of standard penetration test (SPT)

Soil	Typical $N$ value	$N$ value	Relative density	USCS
Fill	3/30	1/30~6/30	Very loose	SM
Weathered soil (Depth < 5 m)	34/30	16/30~46/30	Medium~Dense	SM
Weathered soil (Depth > 5 m)	50	50/30~50/13	Very dense	SM
Weathered soil	50	50/14~50/11	Very dense	-

Table 4 Results of borehole shear test (BST) at G.L. (-) 4 m

Borehole No.	Type	Friction angle ( $^{\circ}$ )	Cohesion (kPa)	Unit weight ( $\text{kN/m}^3$ )
BH-1	Weathered soil (SM)	34.2	0.13	19.0
BH-2	Weathered soil (SM)	30.8	0.23	19.0
BH-3	Weathered soil (SM)	31.4	0.22	19.0
Average		32.1	0.19	19.0

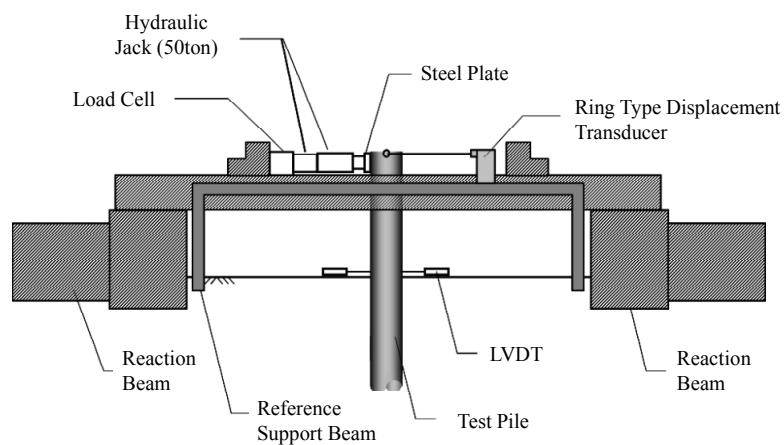


Fig. 5 A schematic representation of the loading system for static load test

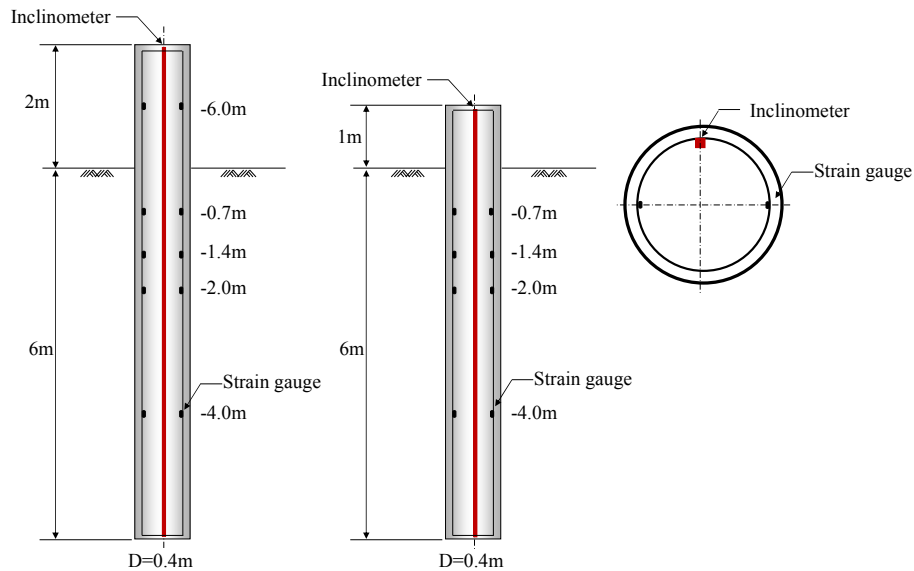


Fig. 6 A schematic representation of the instrumented piles

Table 5 Instrumentation used in field test

	Type	Total quantity	Note
Strain gauge	Vibration wire type	$6 \times 12$	-
Inclinometer	Manual type	1	-
Ring type displacement meter	Electrical type	1	Two-way $\pm 50$ cm
LVDT	Electrical type	3	Surface: 2 Reference beam: 1
Load cell	Electrical type	2	-

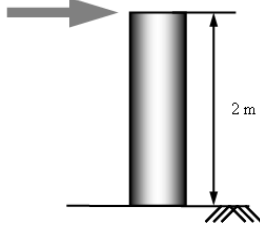
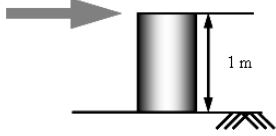
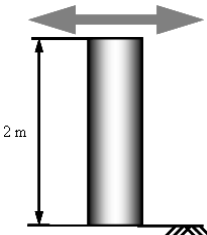
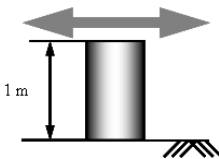
maximum capacity of the hydraulic jack was 500 kN. A schematic representation of an instrumented pile is shown in Fig. 6. This study utilized automated equipment for cyclic load testing that included electrical resistance strain gauges, linear variable differential transformers (LVDTs), inclinometers and ring type displacement meters. A total of 12 electrical resistance strain gauges and 2 LVDTs were attached to the test pile. Table 5 summarizes the instrumentation used in field test.

### 3.3 Cyclic lateral load tests

In this study, full-scale field cyclic load tests were performed on six instrumented piles. Six full-scale drilled shaft piles (400-mm diameter) were tested under either one-way cyclic lateral loading or two-way lateral loading and Table 6 summarized the types of test piles.

As shown in Fig. 7, test piles LTP-1 and LTP-4 were subjected to one-way cyclic loading, while LTP-2, LTP-3, LTP-5 and LTP-6 were subjected to two-way cyclic loading. The test piles LTP-1, LTP-2 and LTP-3 consisted of a column extending 2 m above ground. LTP-4, LTP-5 and LTP-6 consisted of a column extending 1 m above ground. The test piles had an outer diameter of

Table 6 Types of test pile

Loading type	Free length = 2.0 m	Free length = 1.0 m
One-way cyclic loading		
	LTP-1	LTP-4
Two-way cyclic loading		
	LTP-2 & LTP-3	LTP-5 & LTP-6

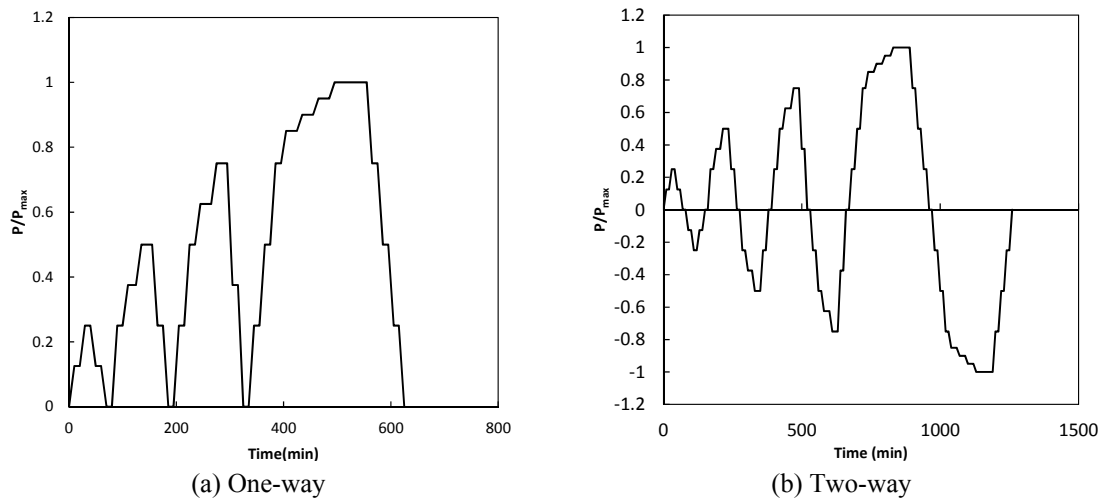


Fig. 7 Cyclic loading sequence

400 mm and embedded length of 6 m. LTP-3 consisted of 6-D16 longitudinal bars and D10 spiral bars at 150 mm spacing. LPT-6 consisted of 6-D16 longitudinal bars and D10 hoop bars at 150 mm spacing.

### 3.4 Comparison with field measurements

In this section, the validation of the numerical analysis against full-scale field test results is discussed. The three-dimensional finite element analysis was conducted using ABAQUS to compare the results of the full-scale field test. The material properties of the soils used in the FE



Table 7 Soil and pile properties in FE analysis (Eumseong case)

	Unit weight (kN/m <sup>3</sup> )	Friction angle (°)	Young's modulus (kPa)	Poisson's ratio
Soil	0~2 m	17.5	17,000	0.3
	2~4 m	18.0	20,500	0.3
	4~6 m	18.5	24,000	0.3
Pile	25.0	-	23,000	0.2

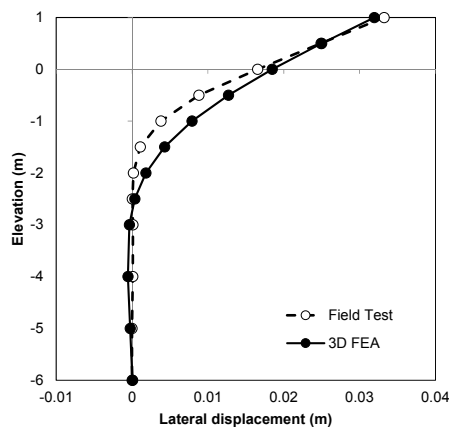
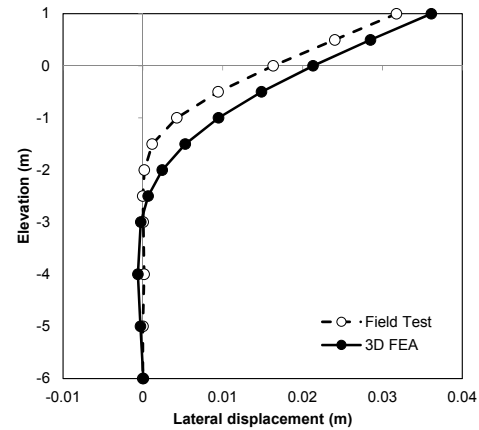
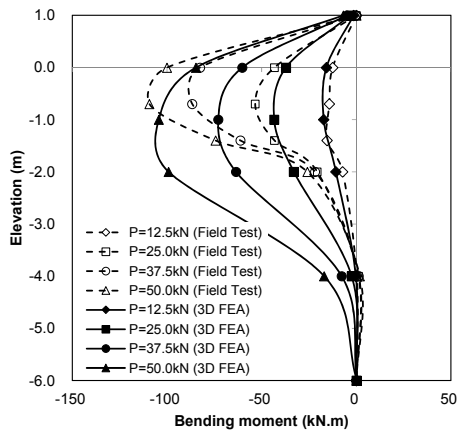
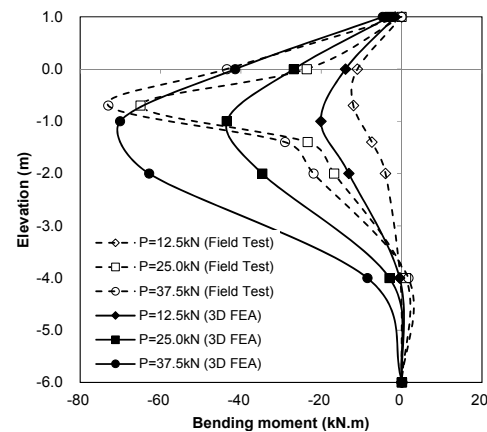
(a) LTP-4 ( $P = 37.5$  kN)(b) LTP-5 ( $P = 37.5$  kN)

Fig. 8 Comparison of computed and measured lateral displacement



(a) LTP-4



(b) LTP-5

Fig. 9 Comparison of computed and measured bending moment

analysis were obtained from the soil investigation. Table 7 shows the soil and pile properties in FE analysis. The loading applied used the same loading conditions as in the field test shown in Fig. 7.

Figs. 8(a) and(b) show the elevation-lateral displacement curves of the test piles LTP-4 and LTP-5 resulting from both and 3D FE analysis. Based on the results, it is clear that the FE analysis

results are capable of predicting the observations of the field test measurements. Figs. 9(a) and (b) show the bending moment of the test piles LTP-4 and LTP-5. Based on the results, it is concluded that the general trend observed by the measurements are similar to the predictions made by FE analysis.

#### 4. Proposed cyclic $p$ - $y$ curve for drilled shafts

##### 4.1 Shapes of $p$ - $y$ curves

Derivations of the experimental  $p$ - $y$  curves using data from fully instrumented lateral load test usually involve mathematics. The soil resistance per unit length ( $p$ ), is calculated by double differentiating the pile bending moment ( $M$ ) distribution (Hetenyi 1946).

$$p = \frac{d^2 M}{dz^2} \quad (4)$$

where  $p$  is net soil resistance per unit length of a pile,  $M$  is bending moment,  $z$  denotes the depth. The lateral pile displacement ( $y$ ), was obtained directly from the measured value or from the double integration of the bending moment profile.

A number of different expressions were considered, such as bilinear, exponential and hyperbolic functions, to match the experimental and numerical analysis  $p$ - $y$  curves. Many researchers (Yang and Liang 2005, Liang *et al.* 2007, Shatnawi 2008) have conducted studies to investigate the hyperbolic functions of  $p$ - $y$  curves based on the goodness of fit with the  $p$ - $y$  curves derived from load test or numerical data.

In this study, general shape of  $p$ - $y$  curve from the numerical analysis the result could be fit mathematically by hyperbolic function. The best fit curve was chosen to be hyperbolic functions of Kondner (1963)

$$p = \frac{y}{\frac{1}{k_h} + \frac{y}{p_u}} \quad (5)$$

where  $p$  (kN/m) is the soil resistance,  $y$  (m) is the lateral displacement,  $k_h$  (kN/m<sup>2</sup>) is the modulus of subgrade reaction and  $p_u$  (kN/m) is the ultimate soil resistance.

The most common initial soil stiffness and ultimate soil resistance used in practice are the values obtained from Vesic (1961) and Broms (1964). In most previous models (Vesic 1961, Ashford and Juirnarongrit 2003), the initial soil stiffness of the  $p$ - $y$  curve is usually estimated from the soil modulus of elasticity,  $E_s$ . This is the basis for the subgrade modulus method in which the soil response is characterized by the coefficient  $k_h$ . Vesic (1961) suggested the following expression (6) based on the analysis of an infinite beam on an elastic foundation

$$k_h = \frac{0.65 E_s}{D(1 - \nu_s^2)} \sqrt[12]{\frac{E_s D^4}{E_p I_p}} \quad (6)$$

where  $E_p I_p$  is the pile flexural stiffness,  $D$  is the width of the pile,  $E_s$  is the soil secant modulus and  $\nu_s$  is the Poisson's ratio of the soil. In  $p$ - $y$  curve analysis, it is common practice to estimate the

ultimate soil resistance by the expressions given by Broms (1964)

$$P_u = 3\left(\frac{1 + \sin \phi}{1 - \sin \phi}\right)\sigma_v \quad (7)$$

where  $\phi$  is the friction angle and  $\sigma_v$  is the vertical stress.

#### 4.2 Cyclic loading conditions

Loading conditions can significantly influence the behavior of piles subjected to cyclic loads. The character of the cyclic load is defined a cyclic load ratio,  $R_H$ . The cyclic loading ratio was proposed by Long and Vanneste (1994) as follows

$$R_H = \frac{P_{\min}}{P_{\max}} \quad (8)$$

where  $P_{\max}$  is the magnitude of the maximum lateral load and  $P_{\min}$  is the magnitude of the minimum lateral load. One-way cyclic loading which is pile cycled from  $P_{\min}$  ( $= 0$ ) to  $P_{\max}$  is calculated to have a cyclic load ratio of  $R_H = 0$ . Whereas a cyclic pile with equal load magnitudes in both directions (two-way loading) would have a value of  $R_H = -1$ , and a pile statically would have a value of  $R_H = 1$ .

To verify the effect of the loading conditions, numerical analyses were performed on the condition in which 40 kN of lateral load was applied. As shown in Fig. 10(b), cyclic loading consists of one-way cyclic loading has a ratio of  $R_H = 0$  and as shown in Fig. 10(a) equal load magnitude in both directions cyclic loading has a ratio of  $R_H = -1$ . Fig. 11 shows that the computed plastic strain in two-way cyclic loading ratio is larger than the one-way loading ratio.

#### 4.3 Proposed cyclic $p$ - $y$ curve and reduction factor

The reduction of initial soil stiffness and ultimate soil resistance was based on full-scale field tests and numerical analysis. The cyclic  $p$ - $y$  curve is related to the hyperbolic  $p$ - $y$  curve in the 3D FE analysis result. In this study, as shown in Fig. 12 the cyclic  $p$ - $y$  curve was proposed by reducing the initial soil stiffness and ultimate soil resistance (9)

$$p = \frac{y}{\frac{1}{C_1 k_h} + \frac{y}{C_2 p_u}} \quad (9)$$

where  $C_1$  and  $C_2$  are reduction factors.

To examine the factors influencing soil properties, a series of FE analyses were performed based on the internal friction angle. The friction angle ranged from 30°-40° in sandy soil. As shown in Fig. 13(a), the lateral displacement occurring between internal friction angles of 30° and 34° was 6 mm, which is 1.5% of the pile diameter at the ground level. As a result, the soil's internal friction angle can significantly influence the behavior of piles. Fig. 13(b) shows the bending moment-depth curves at various internal friction angles. As the internal friction angle increases, bending moments are decreased. Table 8 summarizes the ratio of lateral displacements

and bending moments with an internal friction angle of  $30^\circ$  on the condition in which 40 kN of lateral load is applied. Fig. 14(a) shows the reduction factors ( $C_1$ ,  $C_2$ ) versus friction angle one-way and as shown in Fig. 14(b), the reduction factors ( $C_1$ ,  $C_2$ ) for two-way cyclic loading.

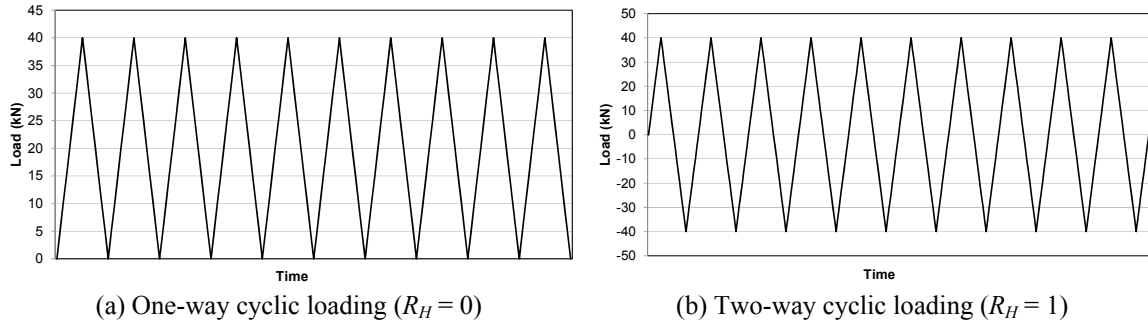


Fig. 10 Loading ratio conditions

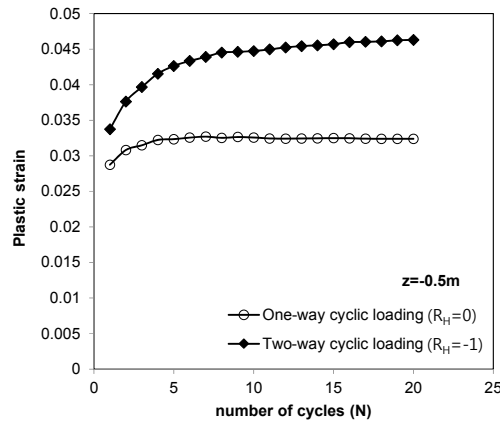


Fig. 11 Comparison of plastic strain curves

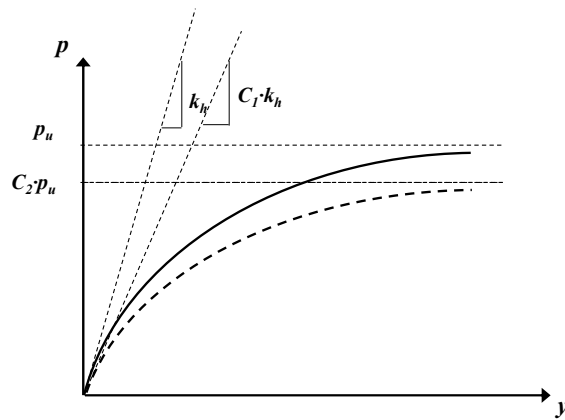


Fig. 12 Concept of proposed  $p$ - $y$  curves for cyclic loading

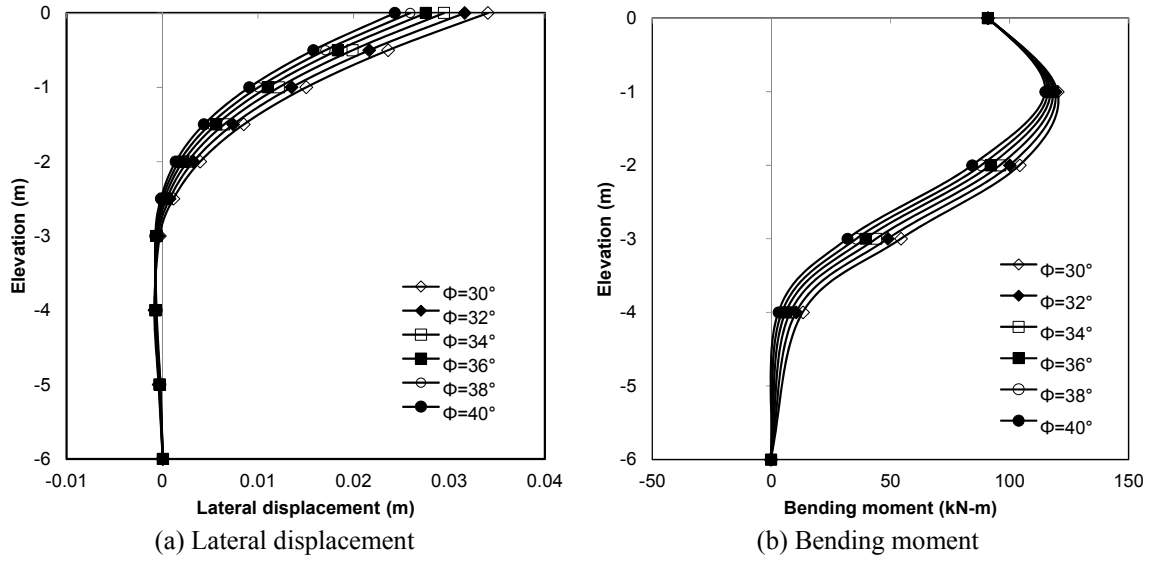


Fig. 13 FE analysis result based on the internal friction angle

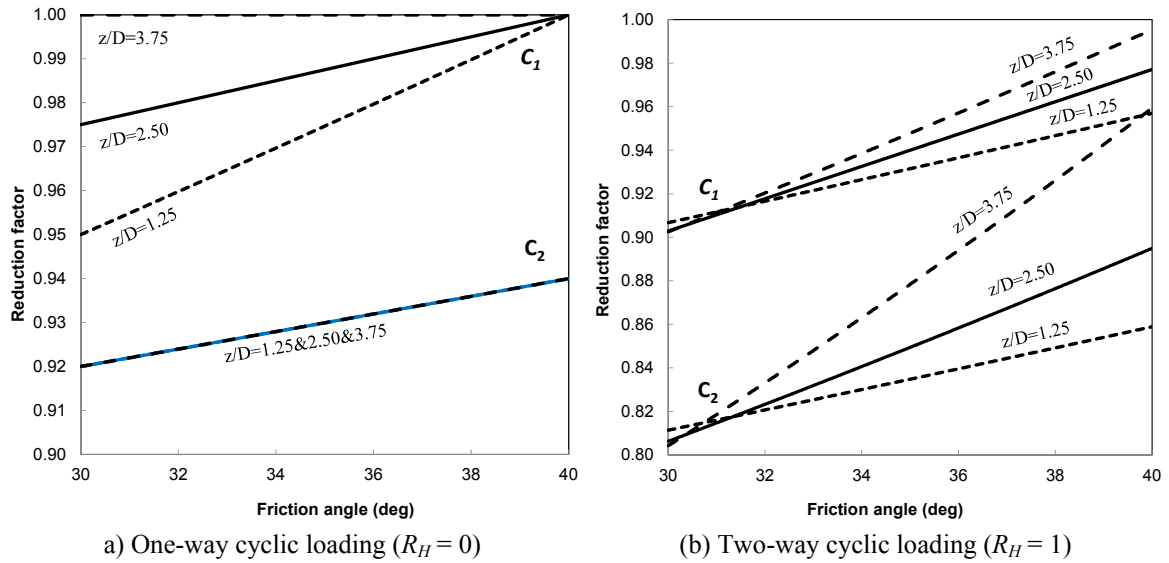


Fig. 14 Reduction factor versus friction angle

Table 8 Lateral displacements and bending moments, according to internal friction angle

	30°	32°	34°	36°	38°	40°
Lateral displacement (mm)	34	31.6	29.4	27.5	25.9	24.3
Ratio (%)	100	92.9	96.5	80.9	76.1	71.4
Bending moment (kN·m)	120.1	119.2	118.25	117.1	116.0	114.9
Ratio (%)	100	99.2	98.4	97.5	96.6	95.7

## 5. Comparison with other case histories

### 5.1 Houston case

The proposed cyclic  $p$ - $y$  curves were validated by comparing the results from the field test and two existing well-known  $p$ - $y$  curves, the API  $p$ - $y$  curve and the Reese  $p$ - $y$  curve, for cyclic loading. The six lateral cyclic loading test on State Highway 146 near Houston, Texas were conducted by Little and Briaud (1988). As shown in Fig. 15, the soil was primarily composed of loose to medium dense fine sand in 22 m underlain by stiff to very stiff clay. This site soil and test pile profile are presented in Fig. 15. To the depth of  $z = (-)1.1$  m, the one-way cyclic loading test pile have calculated reduction factors of  $C_1 = 0.95$ ,  $C_2 = 0.92$  from Fig. 14. The initial soil stiffness and ultimate soil resistance were calculated by Eqs. (6) and (7). Fig. 16 shows the predicted and measured lateral displacement in test piles. The resulting proposed  $p$ - $y$  curves can give good predictions of the measured displacement compared with the API  $p$ - $y$  curve (2005) and the Reese  $p$ - $y$  curve (1974).

### 5.2 California case

Chai and Hutchison (2002) have conducted four full scale ( $D = 406$  mm) reinforced concrete piles embedded in two different soil conditions: loose dry sand ( $\phi = 37^\circ$ ) and dense dry sand ( $\phi = 42^\circ$ ). In order to variation of soil density, free length of pile  $2D$  and  $6D$  ( $D =$  diameter of the pile) were conducted to investigate the influence of the bending moment gradient on the pile curvature distribution. The test pile was embedded in a large soil container diameter of 6.71 m and a depth of 5.49 m and the embedded length of the pile was  $13.5D$ . The lateral force on the pile was provided in axial force applied ( $P = 455$  kN) by a long-stroke double-acting actuator reacting against

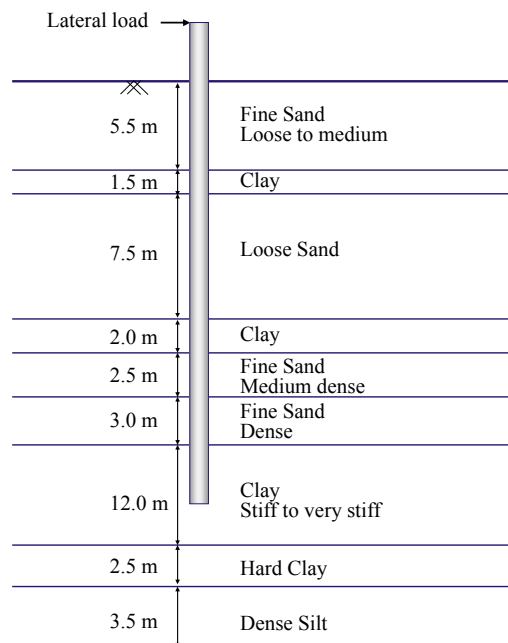


Fig. 15 Soil profile and test piles (Houston case)

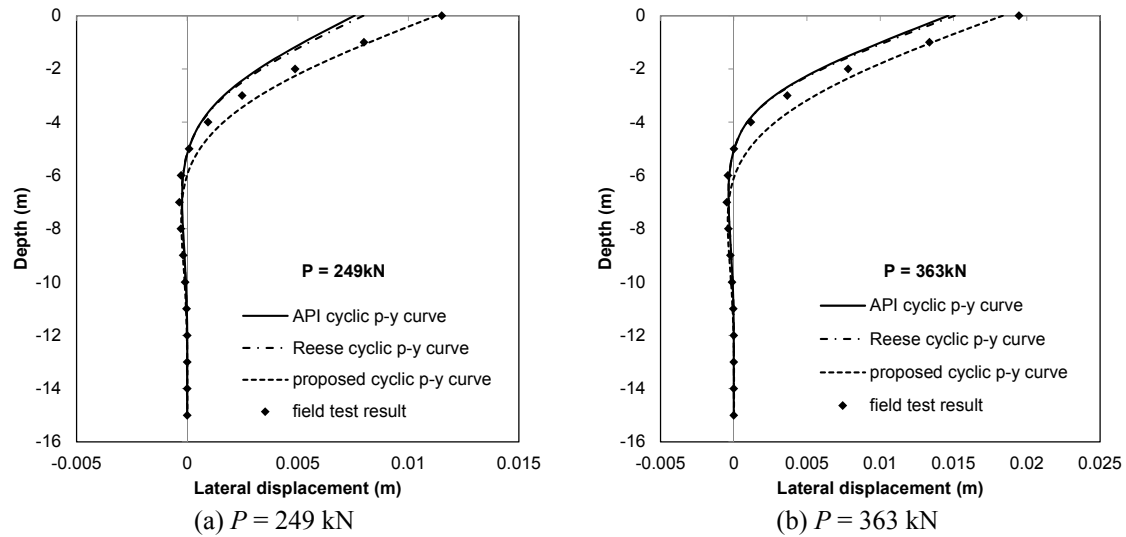


Fig. 16 Comparison of lateral displacement (Houston case)

a large-capacity reaction block. A soil and test piles profile are presented in Fig. 17. In this study, the proposed cyclic  $p$ - $y$  curves were validated by comparing the results from the loose sand condition. To the depth of  $z = (-)0.5 \text{ m}$ , the Two-way cyclic loading ( $R_H = -1$ ) test piles have calculated reduction factors of  $C_1 = 0.94$ ,  $C_2 = 0.84$ , and the reduction factors have calculated of  $C_1 = 0.96$ ,  $C_2 = 0.87$  at depth of  $z = (-)1.0 \text{ m}$  from Fig. 14. Fig. 18 shows the predicted and measured lateral displacement in test piles with a free length of pile  $2D$  and  $6D$ . The resulting proposed  $p$ - $y$  curves can give good predictions of the general trend of the measured displacement compared with the existing  $p$ - $y$  curves.

## 6. Conclusions

The main objective of this study is to quantify the cyclic  $p$ - $y$  curve function from lateral cyclic loading tests and three-dimensional finite element analysis. Full-scale field tests and numerical analysis were conducted to investigate the behavior of drilled shafts.

Based on the findings of this study, the following conclusions can be drawn:

- In this study, a lateral cyclic load transfer relationship and design chart for drilled shafts in weathered soil was proposed by considering the characteristics of cyclic loading based on field tests and numerical analysis.
- To validate the 3D finite element modelling, the field tests under cyclic lateral loading were performed on six instrumented piles. Based on the comparison between the results of numerical analyses and field load tests, it is clear that the FE analysis results are capable of predicting the observations of the field test measurements. Thus, it is concluded that the general trend observed by the measurements are similar to the predictions made by FE analysis.
- To examine the factors influencing soil properties, a series of FE analyses were performed based on the internal friction angle. As a result, the cyclic behavior of piles depends on the

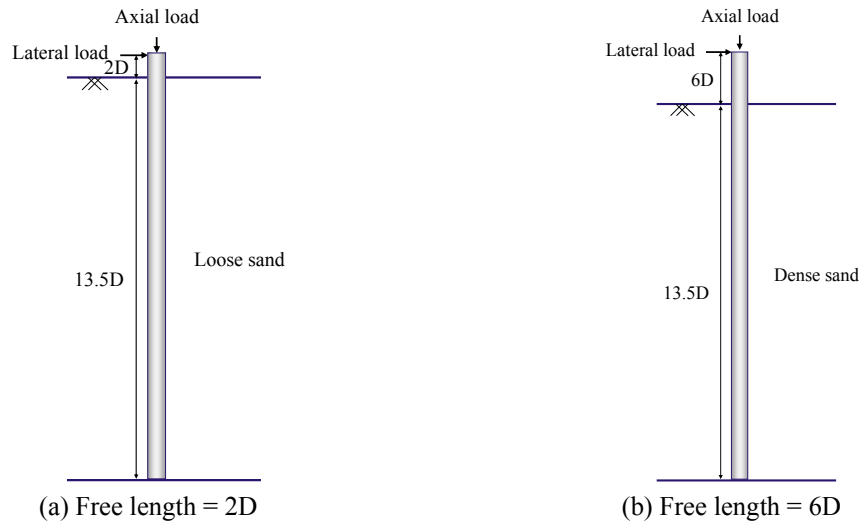


Fig. 17 Soil profiles and test piles (California case)

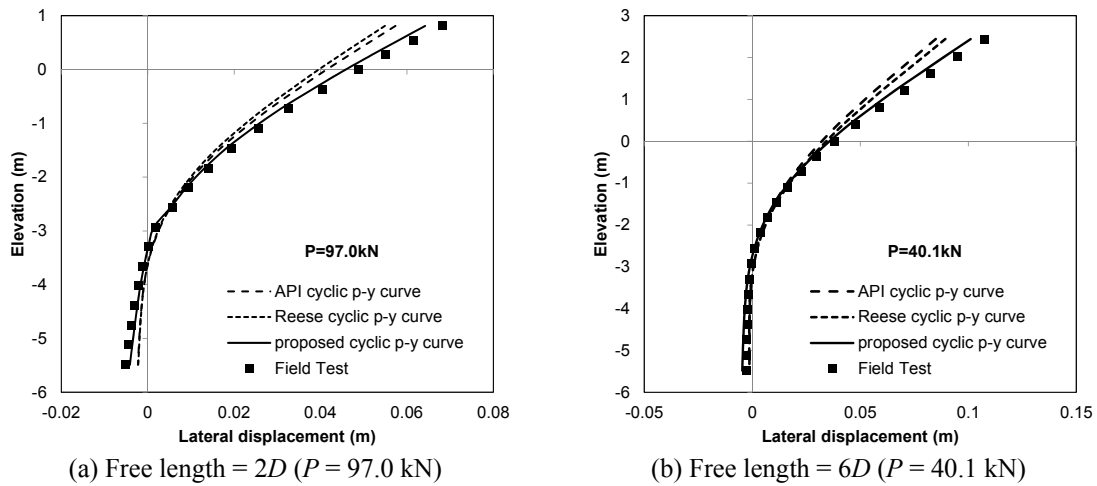


Fig. 18 Comparison of lateral displacement (California case)

internal friction angle. Additionally, as the internal friction angle increased, ultimate soil resistance decreased in both one-way and two-way loading condition. However, the ultimate soil resistance was lower in one-way cyclic loading. Based on the results of parametric studies, the reduction factors ( $C_1$ ,  $C_2$ ) with internal friction angles for one-way and two-way cyclic  $p$ - $y$  curves are proposed, respectively.

- The cyclic  $p$ - $y$  curves using the reduction factors ( $C_1$ ,  $C_2$ ) were validated by comparing the results from the field test (i.e., Houston and California case) and existing  $p$ - $y$  curves (i.e., API model and  $p$ - $y$  curve proposed by Reese). Based on the validation, the proposed cyclic  $p$ - $y$  curve is shown to be capable of predicting the behavior of the drilled shafts in weathered soil. Therefore, the proposed cyclic  $p$ - $y$  curve, which considers the characteristics of cyclic loading, can overcome the limitations of the existing empirical  $p$ - $y$  curves.



## Acknowledgments

This work was supported by the National Research Foundation of Korea (NRF) grant funded by the Korea government (MSIP) (Grant Nos. 2011-0030040 and 2016R1A6A3A03010454).

## References

- ABAQUS (2013), Analysis user's manual, Version 6.13; Published by Hibbit, Karlsson and Sorensen Inc., USA.
- Achmus, M., Kou, Y.S. and Abdel-Rahman, K. (2009), "Behavior of monopile foundations under cyclic lateral load", *Comput. Geotech.*, **36**(5), 725-735.
- American Petroleum Institute (2005), Recommended Practice for Planning, Designing and Constructing Fixed Offshore Platform-Working Stress Design: API Recommended Practice 2A-WSD Twenty-first Edition.
- Ashford, S. and Juirnarongrit, T. (2003), "Evaluation of pile diameter effect on initial modulus of subgrade reaction", *J. Geotech. Geoenviron. Eng.*, **129**(3), 234-242.
- Ashour, M. and Norris, G. (2000), "Modeling lateral soil-pile response based on soil-pile interaction", *J. Geotech. Geoenviron. Eng.*, **126**(5), 420-428.
- Bourgeois, E., Rakotonindriana, M.H.J., Kouby, A.L. and Serratrice, J.F. (2010), "Three-dimensional numerical modelling of the behaviour of a pile subjected to cyclic lateral loading", *Comput. Geotech.*, **37**(3), 999-1007.
- Broms, B. (1964), "Lateral resistance of piles in cohesionless soils", *J. Soil Mech. Foun. Div.*, **90**(3), 123-158.
- Chai, Y.H. and Hutchinson, T.C. (2002), "Flexural strength and ductility of extended pile-shafts. II: Experimental study", *J. Struct. Eng.*, **128**(5), 595-602.
- Damgaard, M., Bayat, M., Andersen, L.V. and Ibsen, L.B. (2014), "Assessment of the dynamic behaviour of saturated soil subjected to cyclic loading from offshore monopile wind turbine foundations", *Comput. Geotech.*, **61**, 116-126.
- Drumm, E.C., Huang, B., He, W. and Zuo, G. (2005), "Back-calculation of rock socket friction for concrete shafts in Karst", *Proceedings of 11th International Conference of the Association for Computers Methods and Advances in Geomechanics*, Torino, Italy, June, pp. 437-444.
- El Naggar, M.H. and Bentley, K.J. (2000), "Dynamic analysis for laterally loaded piles and dynamic p-y curves", *Can. Geotech. J.*, **37**(6), 1166-1183.
- Hassan, K.H. and O'Neill, M.W. (1997), "Side load transfer mechanisms in drilled shafts in soft argillaceous rock", *J. Geotech. Geoenviron. Eng.*, **123**(2), 145-152.
- Hetenyi, M. (1946), *Beams on Elastic Foundation*, The University of Michigan Press.
- Kim, Y.H. and Jeong, S.S. (2011), "Analysis of soil resistance on laterally loaded piles based on 3D soil-pile interaction", *Comput. Geotech.*, **38**(2), 248-257.
- Kim, G.R., Park, D.G., Kyung, D.H. and Lee, J.H. (2014), "CPT-based lateral displacement analysis using p-y method for offshore mono-piles in clays", *Geomech. Eng., Int. J.*, **7**(4), 459-475.
- Kim, G.R., Kyung, D.H., Park, D.G. and Lee, J.H. (2015), "CPT-based p-y analysis for mono-piles in sands under static and cyclic loading conditions", *Geomech. Eng., Int. J.*, **9**(3), 313-328.
- Kondner, R.L. (1963), "Hyperbolic stress-strain response: Cohesive soils", *J. Soil Mech. Foun. Div.*, **89**(1), 115-144.
- Liang, R., Shatnawi, E.S. and Nusairat, J. (2007), "Hyperbolic p-y criterion for cohesive soils", *Jordan J. Civil Eng.*, **1**(1), 38-58.
- Lin, S.S. and Liao, J.C. (1999), "Permanent strains of piles in sand due to cyclic lateral loads", *J. Geotech. Geoenviron. Eng.*, **125**(9), 798-802.
- Little, R.L. and Briaud, J.L. (1988), *Full Scale Cyclic Lateral Load Tests on Six Single Piles in Sand*, US

- Army Corps of Engineers.
- Liu, J., Zou, D. and Kong, X. (2014), "A three-dimensional state-dependent model of soil-structure interface for monotonic and cyclic loadings", *Comput. Geotech.*, **61**, 166-177.
- Long, J.H. and Vanneste, G. (1994), "Effects of cyclic lateral loads on piles in sand", *J. Geotech. Eng.*, **120**(1), 225-244.
- Matlock, H. (1970), "Correlation for design of laterally loaded piles in soft clay", *Proceedings of the 2nd Annual Offshore Technology Conference*, Houston, TX, USA, April, pp. 577-607.
- McCarron, W.O. (2016), "Bounding surface model for soil resistance to cyclic lateral pile displacements with arbitrary direction", *Comput. Geotech.*, **71**, 47-55.
- Memarpour, M.M., Kimiaei, M., Shayanfar, M. and Khanzadi, M. (2012), "Cyclic lateral response of pile foundations in offshore platforms", *Comput. Geotech.*, **42**, 180-192.
- Murchison, J.M. and O'Neill, M.W. (1984), "Evaluation of  $p$ - $y$  relationships in cohesionless soils", *Proceedings of Analysis and Design of Pile Foundations*, San Francisco, CA, USA, October, pp. 174-191.
- National Cooperative Highway Research Program (2001), NCHRP Report 461-Static and dynamic lateral loading of pile groups.
- Reese, L.C., Cox, W.R. and Koop, F.D. (1974), "Analysis of laterally loaded piles in sand", *Proceedings of the 6th Annual Offshore Technology Conference*, Houston, TX, USA, May, pp. 473-484.
- Shatnawi, E.S. (2008), "Development of  $p$ - $y$  criterion for anisotropic rock and cohesive intermediate geomaterials", PhD thesis; University of Akron, OH, USA.
- Verdure, L., Garnier, J. and Levacher, D. (2003), "Lateral cyclic loading of single piles in sand", *Int. J. Phy. Model. Geotech.*, **3**(3), 17-28.
- Vesic, A.B. (1961), "Beams on elastic subgrade and the Winkler's hypothesis", *Proceedings of 5th International Conference on Soil Mechanics & Foundation Engineering*, Paris, France, July, pp. 845-850.
- Yang, K. and Liang, R. (2005), "Lateral response of large diameter drilled shafts in clay", *Proceedings of 30th Annual Conference on Deep Foundations*, Deep Foundation Institute, Chicago, IL, USA, September, pp. 115-126.
- Yang, E.K., Jeong, S.S., Kim, J.H. and Kim, M.M. (2009), "Dynamic  $p$ - $y$  backbone curves from 1 g shaking table tests", *Proceedings of TRB 2009 Annual Meeting*, Washington, D.C., USA, January, pp. 1-16.